Numerical Modeling of Electron Beam Welding in Precipitation Hardened CuCrZr Alloy

A Dissertation Report

Submitted in partial fulfillment of requirements for the degree of

Master of Engineering

In

CAD/CAM Engineering

By

Rajveer Singh

Registration No.:801784014

Under the Supervision of

Dr. Sachin Singh & Dr. P. K. C. Kanigalpula

(Assistant professor, Mechanical Engineering Department)

MECHANICAL ENGINEERING DEPARTMENT

THAPAR INSTITUTE OF ENGINEERING &TECHNOLOGY, PATIALA

July, 2019

Candidate's Declaration

I hereby declare that the dissertation entitled "**Numerical Modeling of Electron Beam Welding in Precipitation Hardened CuCrZr Alloy**" is an authentic record of my work carried out as requirements for the award of the degree of **Master of Engineering** in **CAD/CAM Engineering** at **Thapar Institute of Engineering and Technology, Patiala** under the supervision of **Dr. Sachin Singh & Dr.P.K.C.Kanigalpula (Assistant Professor, Mechanical Engineering Department).** No part of the matter embodied in this report has been submitted to any other university or institute for the award of any degree.

Date: 31-July-2019

Rajveer singh
Roll No.801784014
Thapar Institute of Engineering and Technology, Patiala

It is certified that the above statement made by the student is correct to the best of my knowledge and belief.

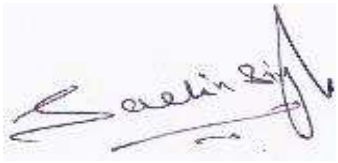

Dr. Sachin Singh
&
Dr. P. K. C. Kanigalpula
Assistant Professor
Mechanical Engineering Department
Thapar Institute of Engineering and Technology, Patiala

ACKNOWLEDGEMENT

I would like to express my special thanks and sense of gratitude to my supervisor Dr. Sachin Singh and co-guide Dr. Dr.P.K.C.Kanigalpula for the guidance. I have been extremely lucky to have supervisor's like them who helped me in my work and I came to know about so many new things. They provided me the technical support, facilities and skills that really helped me during the work. They cared so much about my work over the year. Their patience, the adjustments they made, and trust and confidence they had in me really helped me to finish my work at the right time.

Furthermore I would like to express my sincere gratitude to the Mechanical Engineering Department, Thapar Institute of Engineering and Technology for the technical support. Finally, I would like to express my sincerest sense of gratitude to my family for their support and love for me, without which this work could not have been possible.

ABSTRACT

Precipitation hardened copper chromium zirconium (PH-CuCrZr) has good mechanical properties, high electrical and thermal conductivity. As a result, thus find its wide application in various industries such as nuclear, aerospace and automotive sectors. One of the specific applications of PH-CuCrZr alloy is in international thermal experimental reactor (ITER) for manufacturing of the first wall and cooling tubes of the diverter. In order to maintain the structural consistency during the welding of PH-CuCrZr alloy components electron beam welding (EBW) process is employed.

In the current work, numerical modeling of EBW process during welding of PH-CuCrZr alloy components has been carried out. A three-dimensional finite element (FE) model is developed to predict the output responses (bead penetration and bead width) as a function of EBW input parameters (beam current, acceleration voltage and weld speed). A combined conical and Gaussian heat source is used to model the deep penetration characteristic of the EBW process. Numerical modelling has been carried out by developing user define function (UDF) in Ansys. Present work illustrates that input power and weld speed has a considerable effect on the EBW output responses (bead penetration, bead width). Simulated results are compared with the experimental results and are in good agreement between the finite element model and experimental results.

TABLE OF CONTENT

LIST OF FIGURES

LIST OF TABLES

CHAPTER 1
INTRODUCTION

Precipitation hardened copper chromium zirconium (PH-CuCrZr) alloy belongs to the group of the alloys that has very high electrical conductivity. As a result this alloy has been considered to be promising material in various industries such as nuclear, aerospace and automotive sectors for joining applications.PH-CuCrZr alloy has been employed for the cooling tubes of the diverter and first wall of the international thermal experimental reactor (ITER) because of its outstanding thermal conductivity [1, 2]. This alloy possesses high conductivity because of very low solubility of Cr and Zr in copper while the outstanding strength is characteristic to precipitation and particle-dispersion strengthening mechanisms [3]. Number of researchers stated that mechanical and electrical properties of welded PH-CuCrZr alloys shows a major decrease in their magnitude due to the residual stresses and weld defects. Also there is a considerable difference of microstructure between the welded joint and base material, [4, 5].Electron beam welding (EBW) comes in the category of most famous fusion processes for the welding of various componentsin aerospace and nuclear industries.EBW can produce welds by means of deeper penetration, narrower bead width and insignificant heat affected zone in comparison with other fusion welding processes [6].

In the current work numerical modeling of EBW process during welding of PH-CuCrZr alloy is carried out. Finite element (FE) model is developed by using Ansys software. Accelerating voltage, beam current and weld speed are used as input parameter during the simulation. Developed FE model predicts temperature, bead width (BW) and bead penetration (BP) as output responses. Results obtained from the simulation are compared with the experimental work and found in good agreement.

1.1Electron-beam welding

The schematic representation of an EBW machine is shown in Fig. 1.1. The main components of an EBW machine are as follows:

1. Electron-beam gun
2. Electro-magnetic (EM)focusing lens and the combination of deflection and oscillation lens
3. Work chamber

4. Vacuum system for electron gun chamber and work chamber
5. High voltage power source
6. Electrical controls for power source, EM lenses, and vacuum systems
7. Beam viewing system
8. Work handling system [NC- control system]

The schematic view illustrates the axis-symmetric triode type gun and column assembly. The triode gun design consists of high voltage power supply connections, cathode (filament), grid cup, anode and vacuum pumping system. The other subassembly components compose of high voltage cable, focusing and deflection coils. All the components positioned in the electron-beam gun column are put up in a gun chamber.

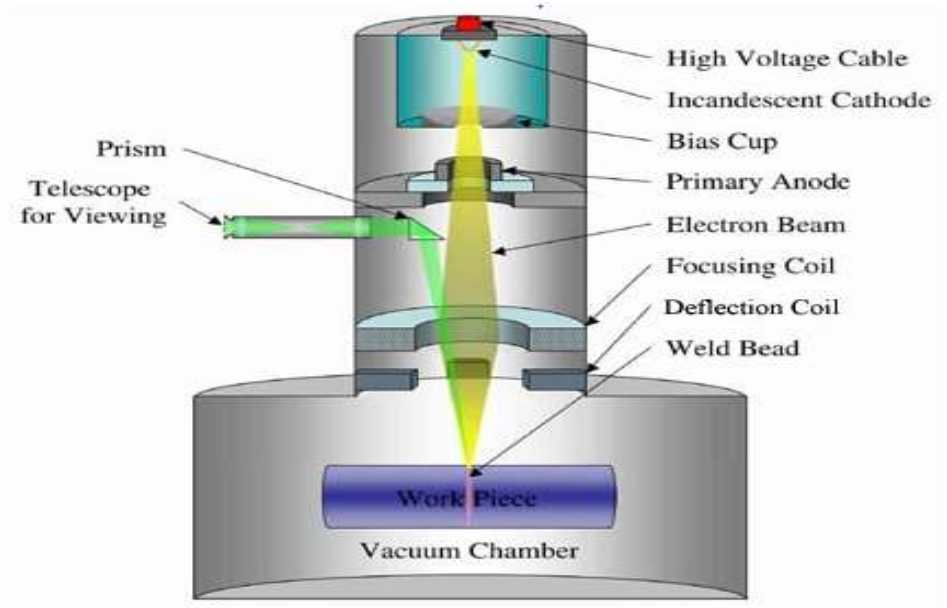

Fig.1.1 *Schematic illustration of an EBW Machine [7]*

1.2 Working principle

During the EBW process electrons are emitted by thermal emission (emission temperature fall normally in the range of 2500 ˚C -2800 ˚C) from a tungsten (W) or tantalum (Ta) cathode and accelerated by an electrostatic field in the direction of the anode [7]. The beam current is controlled by a control electrode (grid cup), which provides the purpose of accelerating and focusing the electron-beam so that the highest beam current (≤ 200 mA) is transmitted through the anode slit. This grid cup is usually negatively biased, as a result that the electrons generated by this cathode do not depart and move towards the next element, anode, in the form of a beam.

The annular anode at this moment attracts the electron-beam and slowly gets accelerated. The characteristic of this electron-beam is divergent in nature at the outlet of the anode.

As electrons depart the anode section, they may attain a velocity as high as half of that of light. This deviating beam is focused through a series of magnetic slits. The magnetic lenses positioned under anode forms the beam and attempt to reduce the divergence. On the other hand, the slits permit only the convergent electrons to bypass through and at the same time confine the divergent low energy electrons from the fringes. Therefore, the slit and magnetic lenses develop the quality of the electron beam. Thereafter, the electron-beam passes throughout the electromagnetic lens and deflection coil. The electromagnetic lens focuses the beam to the required spot to attain high power density required for welding. The deflection coil can deflect the electron-beam by a very small amount, such that the energy transfer takes place in almost proper position inside this field with the lateral uniform division of energy, which results into the enhanced shape of the weld profile.

Electron-beam (EB) comprises of charge carriers (electrons) accelerated by a potential difference in the range of tens of kilovolts. Electrons have a speed equal to two-third of that of the light, and therefore, it has a very high kinetic energy. When these energetic electrons hit the surface of the work piece, a significant section of their kinetic energy is transformed into heat, when the beam impinges at the target surface the electron encounters resistance from the lattice, causing a progressive drop off in its velocity, until it finally comes to rest. The energy of the impinging electrons is shifted to the lattice electrons, which, sequentially increases the vibrational energy of the whole lattice and as a result, heating of the material takes place [8] to evaporation temperature and metal vapor is produced with a very high pressure in that small volume. The outline of the capillary formed by the beam will be determined by the balance of the forces generated by the vapor pressure on one end, and the surface tension and hydrostatic pressure of the molten metal on the other. If the power density of the incident beam is sufficient then the vapor cavity remains and the area for the beam accomplishment shifts in the direction of the deeper level of plate thickness.

1.3 Advantages of the electron beam welding

Following are the major advantages of EBW process:

- **Minimal distortion and shrinkage:** Due to very narrow spot size generated during EBW process it leads to minimum distortion and shrinkage of the component with a very narrow heat affected zone.
- **No gas contamination:** EBW process is performed in the vacuum hence there is no gas contamination during the welding that results in very clean and high-quality weld. EBW is the best option for the parts that required post weld testing process. This application of vacuum allows welding of such materials which are highly reactive with atmospheric gases. In case of other advance welding like laser beam welding (LBW), tungsten inert gas welding (TIGW), and metal inert gas welding (MIGW) etc., no such arrangement of vacuum so there are chances that metal can react with the atmospheric gases.
- **High thickness components:** Due to small focal spot diameter (0.1 – 5 mm), EBW has high power density of around 106 W/cm^2. As a result, EBW process has a potential to join large thicknesses (0.025mm to 100 mm) components in a single pass.
- **High efficiency:** The efficiency of EBW is around 80% to 95 %.

The only drawback of EBW is that there is a size limit for the work piece it can only weld the material that can come or fit in its vacuum chamber not bigger than that of the vacuum chamber size.

1.4Application of the electron beam welding

EBW process finds its wide applications in various industrial sectors due its accuracy and low distortion in the welded component. During EBW process, control of the welding spot size can be achieved easily with the help of magnetic coils.

Industries where the EBW is having very wide applications are as follows:

- **Aerospace industry:** In the aerospace industry there are various components which are electron-beam welded such as, compressor (Fig. 1.2) rocket engine actuators, turbine blades (Fig. 1.3) and the air frames etc. [9].

Fig. 1.2 *Compressor rotor welding[web source]*

Fig. 1.3 *Turbine blade repair[web source]*

- **Oil and Gas industry**: In these industries the weld joint required to maintain the high strength and corrosion resistancefor the oil and the highly reactive gases. Hence, the EBW process provides the best quality. Impeller is the main and the base part of the oil and gas industries and the joining of cover to the impeller is accomplished by means of the EBW process (Fig. 1.4).
- **Automotive industry:** In this industry the synchronization of the multiple gears is done with the help of EBW. Mainly the transmission components of automobile parts are welded by means of EBW process.

Fig.1.4 *Turbocharger impeller welding [web source]*

- **Power generation industry:** The cover of the combustion chamber used in the power generation is welded with the help of EBW process.
- **Defense industry:** Transmission components of the heavy-duty fighting jet are modeled by EBW process.
- **Medical industry:** In the medical the orthopedic welding is accomplished by means of EBW process (Fig. 1.5).

Fig. 1.5 *Orthopedic implant welding [web source]*

CHAPTER 2
LITERATURE REVIEW

Various research works carried out in the field of EBW process can broadly classify in following three broad categories:

2.1 Experimental study

Experimental and theoretical work has been done onTi6A14Vand 21Cr6Ni9Mn alloy to measure the temperature distribution during the EBW [10]. Output response of the model includes velocity fields and temperature. The numerically simulated fusion zone (FZ) geometry and the temperature were compared with experimentally determined outputs of each weld. Both the numerically simulated and experimental results were compared with the output responses for the keyhole mode in laser beam welding (LBW). EBW was done on Al alloy in concern with the heat dissipation through the boundaries of the material, conduction and radiation both the heat transfer modes were considered. The main objective in the present was to control the structural deformation in the AL alloy [11]. The concept of partial penetration in case of EBW was examined [12]. Zhang et al. [13] investigated the effect of different filler metals on the material properties during EBW.Weglowski et al. [14] proposed that EBW process can be used for various applications like coating, rapid prototyping etc. Kaur et al. [15] conducted the experimental and numerical analysis of EBW to join two dissimilar metals alloy. Authors compared the output responses predicted by simulation with the experimentally achieved results**.** Experiments were carried out to check the influence of filler materials on Ti6A14V material weldment in case of EBW [16] and found that effect was in a considerable amount in terms of its geometry and on its microstructure. Sun and karppi [17] further showed that high power density and control over the beam size during EBW process aids in producing good welding in between dissimilar metals. The correlation between outputs parameters (distortion, temperature distribution and weld depth etc.) of EBW process to the thermal efficiency etc. were studied [18, 19, and 20].

2.2 Theoretical study

Wei and Chow [21] proposed an analytical model to compare the various parameters like temperature field around the keyhole and pool geometry with the experimental results. Authors assumed the shape of electron beam following the Gaussian distribution. A 2D mathematical

model was proposed to analyze the various results like heat transfer, keyhole dynamics and the fluid flow during the EBW of Al 2219 aluminum alloy. To predict the penetration depth effect of the keyhole an adaptive heat source model was developed. Authors concluded that results predicted by using adaptive heat source are in good agreement with experimental results [22, 23]. Rouquette et al. [24] proposed the work to analyze the heat source model along the longitudinal section in EBW. Finding the Gaussian parameter terms like energy distribution in the welded zone was the main aim of this work. Hemmer and Grong [25] proposed an analytical model to predict the penetration depth by combining the moving line source and cylindrical cavity for the material like high strength steel, aluminum. A study was carried out by Elmer et al. [26] to correlate the relationship between energy densities and the shape of the weld source. Authors concluded that for energy value above a threshold the weld source behaves as point source else behave like a line source for low energy density. Experimentally it is highly difficult to measure the temperature around the keyhole developed during the EBW process. To overcome such limitations authors proposed an analytical 3-D model to estimate the temperature distribution around the keyhole. In their work they have assumed beam the shape of the keyhole was parabolic and the input power of the EBW was followed Gaussian distribution. To find the analytical solution, parabolic coordinate was utilized [27]. Turygin et al. [28] proposed an algorithm to join the complex parts during the EBW process. Developed algorithm controls the beam movement with accuracy to follow the complex path to be weld.

2.3Numerical study

The numerical study of EBW process helps in the prediction of various output responses such as weld pool geometry, temperature field around the keyhole, residual stresses and distortion of the weld plate. Authors carried out a transient thermal analysis during the EBW of steel tubes. Results obtained after the thermal analysis used as input to carried out the mechanical analysis [29]. Authors predicted the temperature field, heat affected zone and the residual stresses produced during the EBW process. The obtained result further allows us to find the material properties like stress and strain. This analysis also allows us to optimize some other process parameter related to welding process such as input power and speed of the welding. ADINA system is used to accomplish this simulation [30].

EBW process is typically employed to join the dissimilar metal parts and the super alloy. The simulation of the butt joint type welded plat made up of Inconel706 was analyzed. Effects of the

welding parameters on the weld pool geometry of the work part were studied. On this butt joint some certain test was carried out such as X-ray diffraction, tensile test, and micro structural analysis. To accomplish all these of test an uncoupled analysis was done. The heat source model was modeled by combining a spherical with a conical shape type heat source model with Gaussian power density distribution to get the result closer to the experimental results [31]. Lacki et al. [32] had done 49 welds on chrome-nickel steel plate by varying the various welding input parameters to find the same results. The shape of heat source model made in this simulation was designed on the basis of geometry of fusion zone.

A 3D model was prepared to examine the residual stresses and the distortion produced in the welded plate during the EBW process. Butt type Welded plate of Inconel718 and Ti-6Al-4V and Nickel-lead and nickel-Tinwere analyzed in the present work. A particular effort was made to find out the input heat power to be given to the welding. The heat source model was prepared by super imposing a conical and a double ellipsoidal heat source model to analyze the penetration depth characteristics of EBW to validate the calculated results and the experimental result. And hence found that by modeling this combine heat source model the result has good agreement with experimental results [33, 34, and 35]. Gery et al. [36] were proposed a 3D model by assuming the double ellipsoid (Goldak heat flux distribution). Temperature field and various required parameters were found out. To implement the heat flux, C++ Programming was done.

Study presents a 3-D FE model to calculate the temperature history and distortion during the EBW of a high strength aluminum alloy plate. A very fine meshing was done to incorporate the heat source model for EBW simulation. A parallel computational was performed to reduce the simulation time. Various parameters of EBW was studied such as the speed of welding and the heat given to the EB welding and also found the impact of these parameters on the weld pool. An ellipsoidal heat source model was prepared for this aluminum material [37].

A studied was carried out on the 304L stainless steel. The EBW process was done at different power densities distributions. The results were observed by fixing the heat input and varying the weld spot radius. Temperature also considered along the depth of the keyhole. Force balanced method was used to calculate the vapor pressure on the wall of the keyhole. This model basically focused to calculate the weld pool geometry and the fluid flow pattern in the electron-beam welding [38].

Authors [39] carried out the study on the magnesium AZ61 alloy. The vacuum electron-beam welding (VEBW), penetration depth, thermal field at fusion zone and the surface thermal outcome of high temperature metal vapor were examine by means of the direct acting method. To accomplish this kind of simulation a new heat source model was developed by combining the Gaussian heat source model and the conical heat source model. Hence the Gaussian heat source model was for the surface thermal field and the conical heat source model was to find the results for penetration depth of the welding. And it was found that the current supply to the heat source model will affect the thermal field of the key hole and the weld shape.

A simulation of EBW process by using a copper coating as the filler material was carried out. The materials which joined by this welding were Ti-15-3 titanium alloy and 304 stainless steel. Simulation was done to examine the temperature field and the distortion produced in the joint during the welding and the result of accomplished simulation later validated with the experimental results and it is found that results are nearly close to the calculated results. According to the results the parabola body heat source model was the best heat source model for this type of welding conditions. Using this parabola heat source model, it was found that all the thermal forces are in asymmetric distribution. In the simulation it was also found that the temperature produced in the Ti alloy is more than that of steel alloy. Hence it was concluded from this papers that copper react as the good filler material in case of EBW process [40].

A study of EBW process by oscillating the beam inside the keyhole was carried out and the impact of the oscillatory beam and its parameters was analyzed. Effect on the shape of the keyhole, various weld parameters and the flow of the heat transfer was also studied. The model was prepared as per the conduction and Navier-stokes heat equations. The keyhole shape was developed with the help of experimental data. The keyhole was developed in this case by superimposing a slanted elliptical cone with a spherical apex [41, 42]. A study of the micro-structure of EB welded plate was done. The materials used in the present analysis were HastelloyC-276 and crystalline Zr metal. In the study, energy dispersive system was used and found that, microstructure of the molten pool was in lamellar form. After getting the result it was clear that there were no welding defects like micro cracks and the voids. Heat affected zone was also found very small. It was observed that after welding the hardness of the mote zone was increased [43, 44].

Effects of using activating flux in the EBW process to enhance the quality of deep penetration. To analyze this, a coating of activating flux was placed on the one part and one part was kept blank (without activating flux). Then the welding was done on both the part to find the effect of activating flux. The results showed that activating flux coating has direct effect on the penetration depth capability of the welding in case of stainless steel. A significant improvement was occurred in the penetration when the welding carried out in the mode of conduction. This paper presents the simulation work on the carbon nanotube to predict the covalent junction and the effect of covalent structure on the mechanical response was considered [45].

2.4 Gaps in Literature

In order to understand and optimize any process it is necessary to understand its physics. As per the literature survey, number of researchers experimentally studied EBW process on the material such as stainless steel (30HGSA, 304L), aluminum alloy (Al 2219), magnesium alloy (AZ61) and titanium alloy (Ti-15-3, Ti6A14V) etc. Very few literatures are available with the experimental study of EBW process during the welding of PH-CuCrZr alloy. Also, no literature is available which deals with its numerical study.

2.5 Objectives

Based on the literature review, the following are the broad objectives of the current work.

1. Numerical analysis by developing FE model of the EBW process during welding of PH-CuCrZr alloy.
2. Developing a heat source model for accurately predicting the output responses of the EBW process.
3. To study the effect of input parameters (beam current, accelerating voltage and weld speed) of EBW process on its output responses (bead width and bed penetration).
4. Comparative study between the experimentally and simulated results.

CHAPTER 3
NUMERICAL MODELING

3.1 Finite element formulation

In the present work a 3D symmetric FE model for transient thermal analysis is developed with the help of commercial ANSYS APDL 14.5 software. The model is having dimensions of 100×25×10 mm^3. Developed model is meshed with a solid 8-noded brick element for the analysis.

3.2 Steps in FE analysis

Steps that constitute the FEM analyses are as follows:

1. Pre-processing
2. Initial and boundary conditions
3. Solution
4. Post processing

Fig. 3.1 depicts sequence of steps followed for performing thermal analysis, as shown in flow diagram a transient thermal analysis is performed by developing the model, meshing followed by applying the proper boundary condition's and material properties. Later, by setting the proper solution controls in Ansys solver simulation is performed. The output results of the simulation are nodal temperature, bead width and bead penetration.

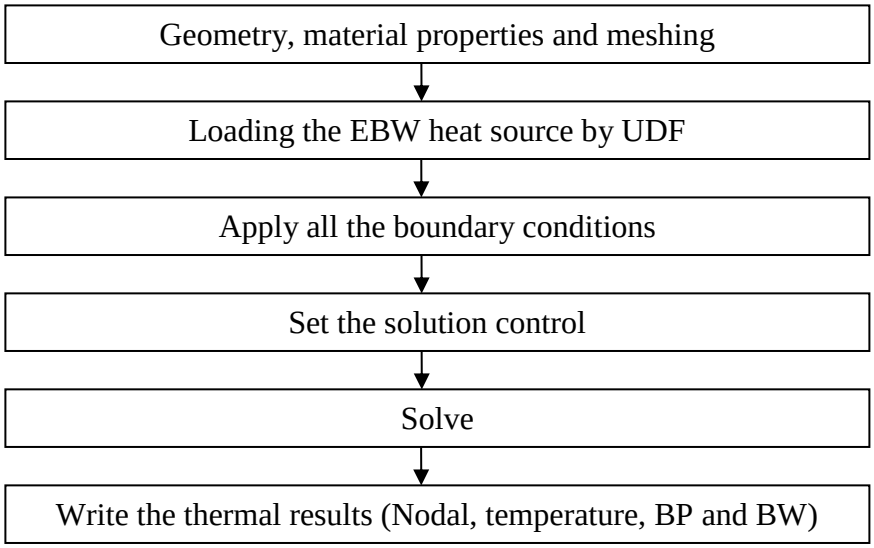

Fig. 3.1*Flowchart for performing thermal analysis*

3.2.1 Pre-processing

Fig. 3.2 shows the two sheet of PH Cu-0.80Rr-0.06Zr alloy to be welded by EBW process along the path A-B-C-D-E-F. The present analysis considers only one sheet A-I-K-C-F-N-L-D by assuming the symmetry of the focused electron beam and the workpiece.

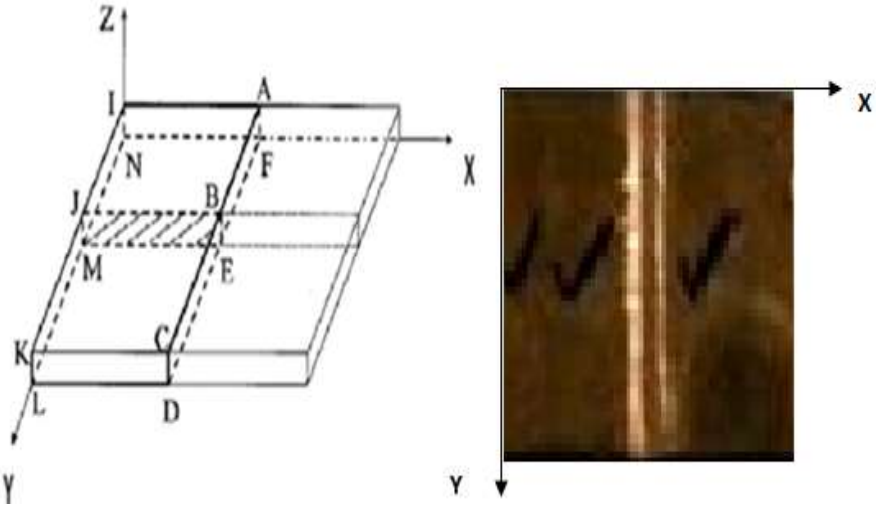

Fig. 3.2 *Schamatic diagram of the developed FE model and original welded specimen.*

3.2.1.1 Meshing

During meshing geometry is discretized into a number of small elements. To perform the mesh convergence, thermal result is compared by meshing the workpiece at different element sizes with same EBW input parameters.

1)During the first run the workpiece is uniformly discretized by solid 8-noded brick element with size of 1 × 1 × 1 mm^3. As shown in Fig. 3.3 temperature varies from a minimum of 300 K to a maximum of 2346.06 K.

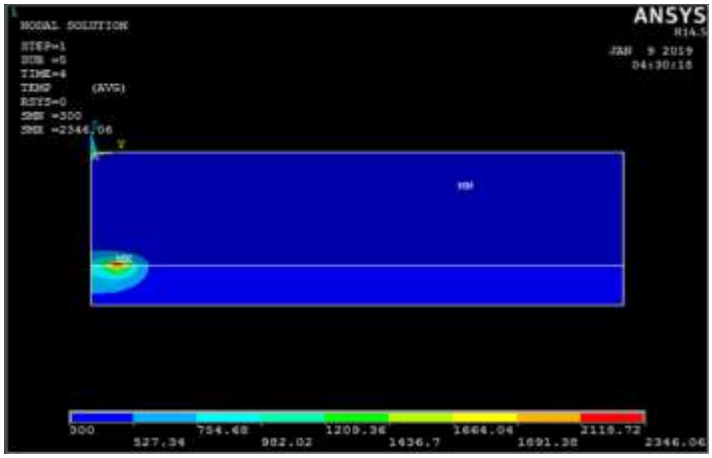

Fig. 3.3 *Nodal temperature value at an elements size of 1 mm each*

2) In the second case, model was uniformly meshed with an element size of 0.5 × 0.5 × 0.5 mm^3. As shown in Fig. 3.4 the maximum temperature rises to 2606.86 K with a difference of 260 K compared with case 1.

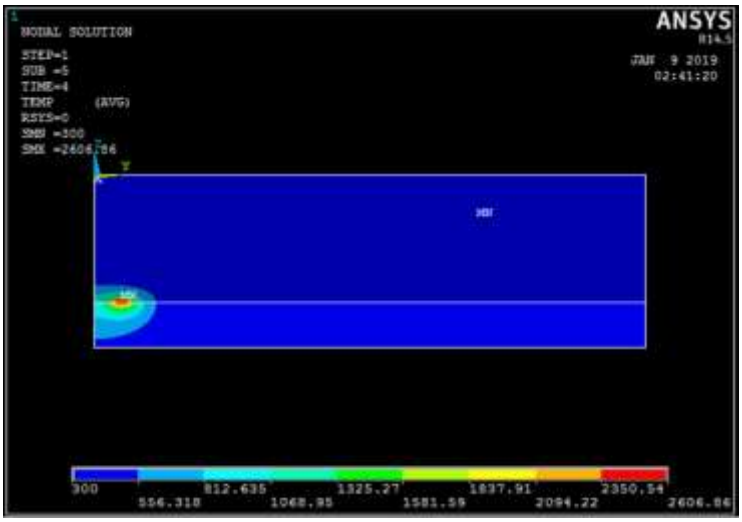

Fig. 3.4 *Nodal temperature value at an elements size of 0.5 mm each*

3)During the third trial the element size was 0.5 × 0.5 × 0.25 mm^3. Maximum temperature achieved is 2625 K (Fig. 3.5). Therefore, the variation between maximum temperature achieved in case 2 and case 3 is negligible.

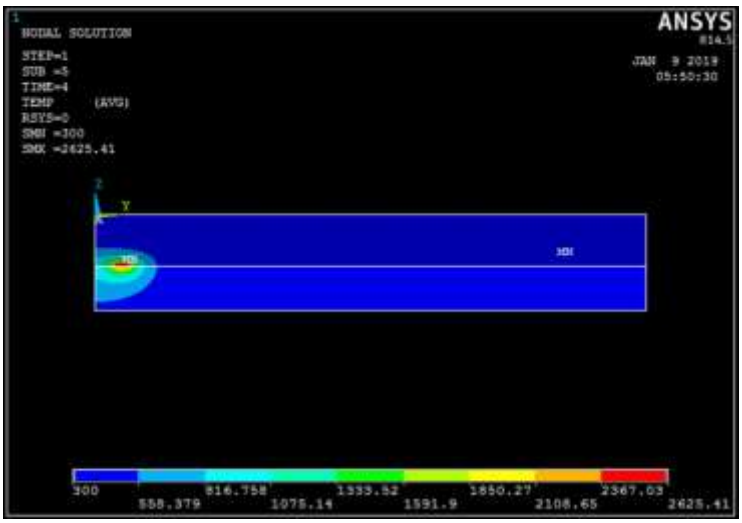

Fig. 3.5 *Nodal temperature value at an elements size of 0.5 mm along the length and 0.25 mm along the thickness side of the model*

As shown in Fig. 3.6, in order to capture the thermal result accurately in the weldment region and simultaneously saving the computational expanses, a fine mesh with element size of 0.5 × 0.5 × 0.25 mm^3 is generated in the weldment region while a coarse mesh with an element size of 1 ×

0.5×0.25 mm^3 is chosen for far of regions. In present analysis211191 nodes and 200000 elements are generated.

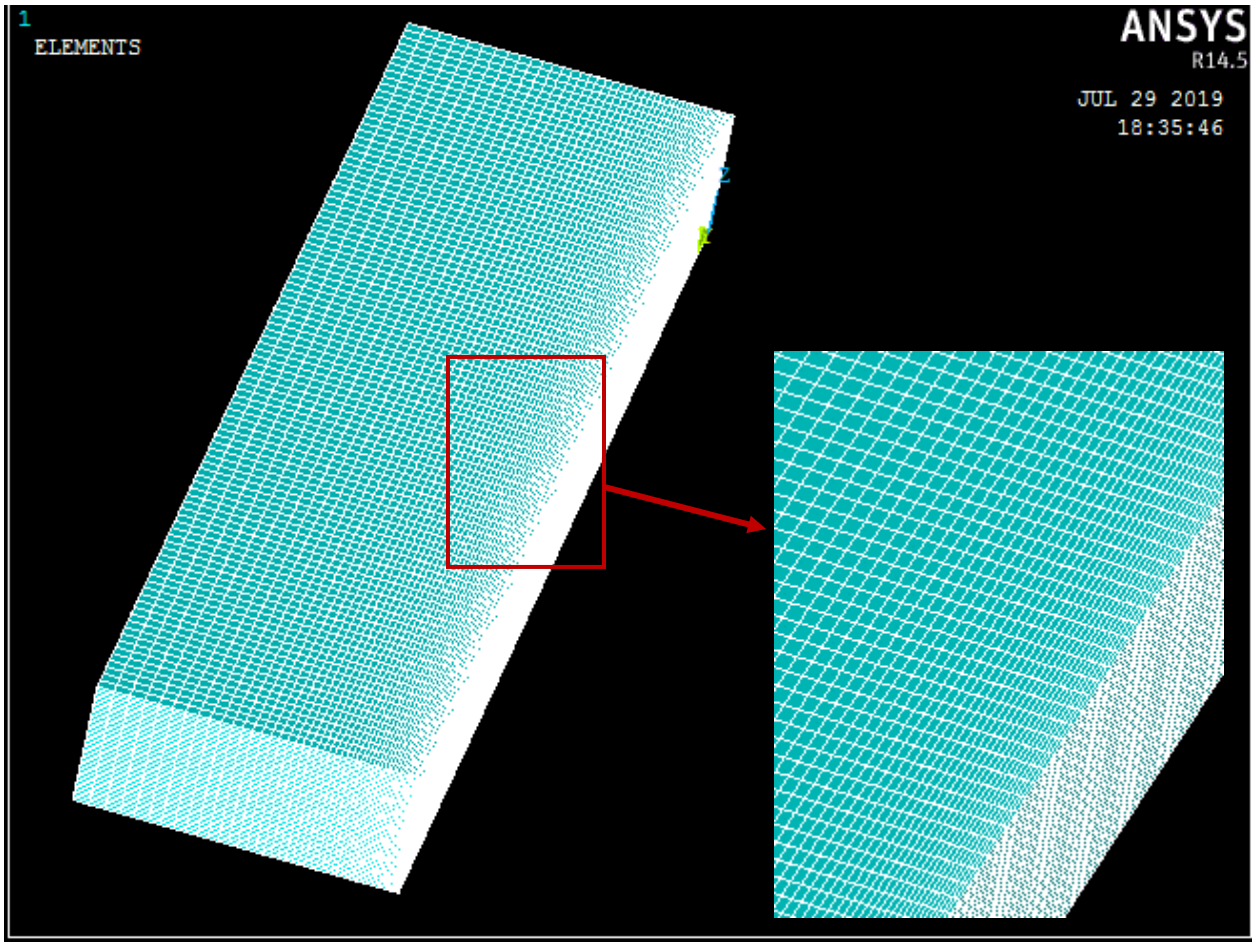

Fig. 3.6 *meshed FE model*

3.2.1.2 Material properties

In order to develop an accurate FE model, temperature dependent material properties are given as input during the simulation. Table 3.1 shows the variation of density, specific heat and thermal conductivity for PH-CuCrZr alloy.

Table 3.1 *Temperature dependent thermal properties of PH-CuCrZr alloy [46]*

Properties	**Temperature (K)**					
	300	**373**	**473**	**573**	**673**	**773**
Density (gcm^{-3})	8.89	8.85	8.81	8.76	8.71	8.66
Specific Heat(J$Kg^{-1}K^{-1}$)	395	404	415	422	431	440
Thermal Conductivity (W$m^{-1}K^{-1}$)	355	358	358	354	350	354

3.2.1.3 Governing equation and heat source model

The 3Dgoverning equation for transient thermal analysis in Cartesian coordinate (*x*, *y* and *z*) is given as:

$$\frac{\partial}{\partial x}\left(k\frac{\partial T}{\partial x}\right)+\frac{\partial}{\partial y}\left(k\frac{\partial T}{\partial y}\right)+\frac{\partial}{\partial z}\left(k\frac{\partial T}{\partial z}\right)+\dot{Q}=\rho C\frac{\partial T}{\partial t} \quad (3.1)$$

Length, width and depth of the workpiece are considered along *x*, *y* and *z* direction. Also, the electron beam moves along the positive *y* direction.

Where,

k = thermal conductivity *(w/mK)*
ρ = density
C = specific heat of material.
T = temperature *(K).*
t= time variable *(s).*
$\dot{Q}$ = internal heat generation rate per unit volume.

To carry out the thermal analysis in the current work beam source is modeled by employing Gaussian distribution followed by conic distribution. As shown in Fig. 3.7 compound heat source model was developed by combining Gaussian and conical heat source model [47]. Various

constant parameters of the heat source are calibrated in the current work in such a way that the simulated results follow the trend and are in a reasonable deviation with the experimental results.

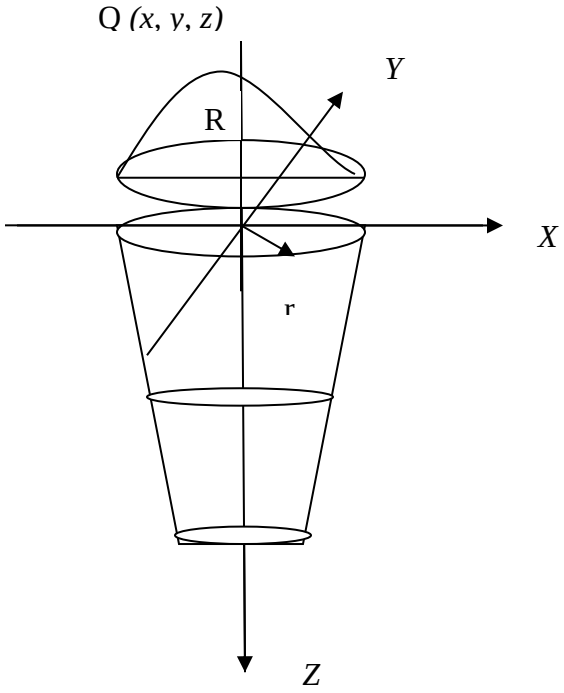

Fig. 3.7*Schematic diagram of the compound heat source model*

Heat generation at a node (*x*, *y*, *z*) is given by equation (2) and (3).

$$q_{Surf}(x,y,z) = \frac{21Q_0}{10\pi hr_o^2}\exp[-3\frac{(x^2+y^2)}{r_0^2}] \quad (3.2)$$

$$q_{Key}(x,y,z) = \frac{21Q_0}{10\pi hr_o^2}\exp[-3\frac{(x^2+y^2)}{r_0^2}\left(1+\frac{z}{h}\right)] \quad (3.3)$$

Therefore, total heat flux applied on the workpiece can be written as:

$$Q_T = q_{Surf}(x,y,z) + q_{Key}(x,y,z) \quad (3.4)$$

Where,q_{Surf} is the heat produced by impinging of accelerated electrons, and vapor flux, q_{key} shows the heat transferred due to vapor and plasma generated by energy input at the bottom of the keyhole. Fig. 3.8 shows the various types of heat flux generated during the EBW process.

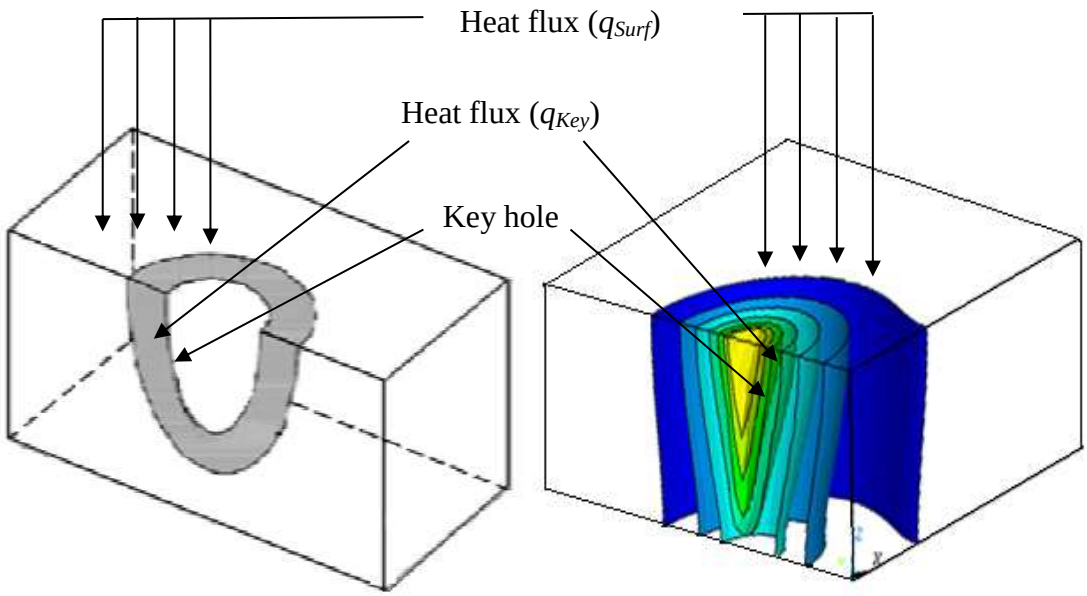

Fig. 3.8 *Schematic with corresponding numerically modeled heat source showing the Gaussian and conical heat flux*

Where, Total heat input $Q_0 = \eta \times V \times I$ in watt *(W).*

η= efficiency of the electron-beam welding machine.

V = voltage supplied in *(kV).*

I= current supplied in *(mA).*

Q= heat flux per unit volume in $[\frac{KW}{m^3}]$.

h= thickness of the work piece *(m).*

r_0 = initial electron-beam radius in *(m).*

3.2.1.4 Initial and boundary conditions

Some of the assumptions taken during the analysis are as follows:

1) The material used in the analysis is assumed as anisotropic continuum,

2) The flow of welding pool was not considered

4) Workpiece was considered with a uniform initial temperature of 300 K,

The boundary conditions used in the present study has a normal conduction (k_n), heat flux (q) and radiation $\sigma\ \varepsilon\ (T^4\text{-}T_0^4)$. Hence the equation of complete boundary conditions can be given as follows:

$$K_n\text{-}q + \sigma\ \varepsilon\ (T^4\text{-}T_0^4) = 0 \qquad (3.5)$$

Where, K_n denotes the thermal conductivity of the material normal to the surface of work piece in W/mK, ε represents the emissivity of surface radiation and σ is the Stefan Boltzmann's constant, which is given by $1.7 \times 10^{-5}\ W/m^2K^4$.

3.2.1.5 Simulating the moving heat source

Weld path is defined by writing the user defined function (UDF) in Ansys parametric design language (APDL) to be followed during the welding simulation. Fig. 3.9 shows the applied heat flux on a three-dimensional model with the help of UDF developed in APDL. Heat flux distribution at a particular load step is calculated by developing a cylindrical local coordinate system at the center of the electron beam. While the heat source model is moved with the help of Cartesian global coordinate system. The radius of the local coordinates system is equal to the initial beam radius, r_0. The weld path consists of applying heat source at various load steps for a particular time step size that are calculated as follows:

$$N_{LS} = \{(L_T - 2 \times r_0) / (S_L)\} \quad (3.6)$$

$$T_{SS} = (S_L / W_S) \quad (3.7)$$

Where,

N_{LS} = Number of load steps
L_T = Total length of model
r_0 = Initial radius of electron beam
S_L = Step length
T_{SS} = Time step size
W_S = Weld speed

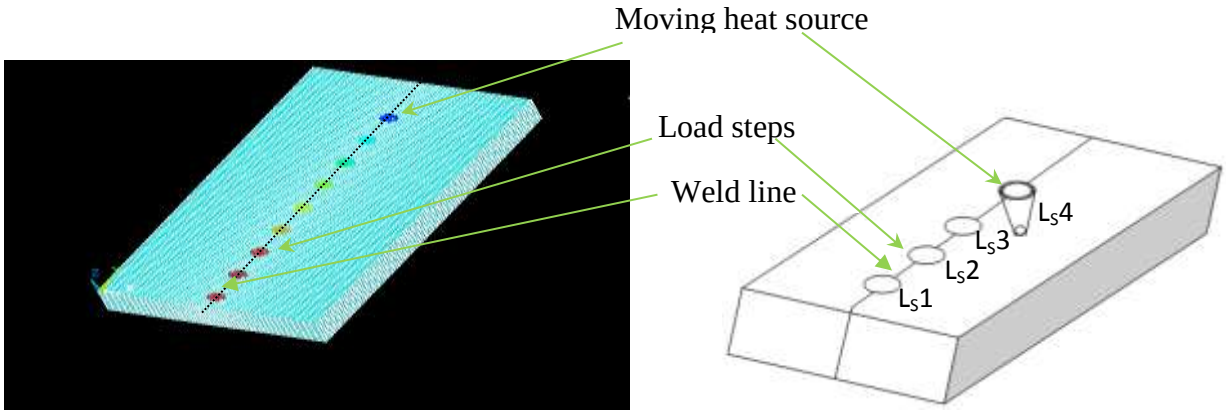

Fig. 3.9*Schematic with Ansys model showing various load steps along the weld path*

Initially, heat flux is applied at various nodes for a particular load step. In the next load step heat source is moved by a step length and heat flux is recalculated for various nodes by deleting the heat flux of the previous load step. This process is repeated along the weld path, thus simulating the moving electron beam during the EBW process.

CHAPTER4

RESULTS AND DISCUSSION

4.1 Thermal analysis of precipitation hardened (PH) CuCrZr alloy (Spot welding)

Initially, for carrying out the numerical study, a code is developed to simulate the spot welding of PH-CuCrZr alloy by EBW process. To accurately capture the shape and size of weld bead *(BP, BW)* at various EBW input parameters Gaussian heat source model and Conical heat source model was employed in the simulation. The whole spot-welding simulation consist two steps one is to apply the heat source model and another is to remove the applied heat source model to cool the weld bead by allowing the heat loss due to conduction only. There is no heat loss due to convection because of the vacuum chamber of the EBW. Fig. 4.1 shows the temperature profile at 70 mA current and voltage of 50 kV applied for 1 second.

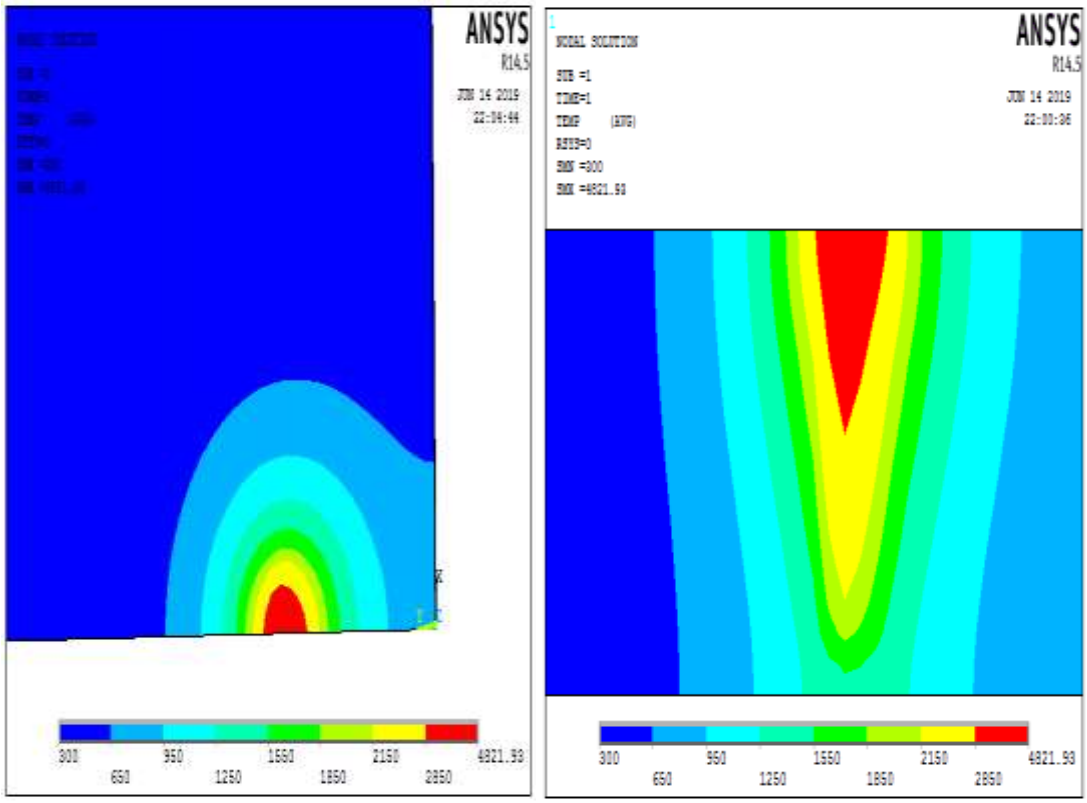

(a) ***(b)***

Fig. 4.1 *Temperature profiles during spot EBW process at the current 70 mA and voltage 50 kV* ***(a)*** *top view* ***(b)*** *side view*

4.2 Thermal analysis of precipitation hardened (PH) CuCrZr alloy (Moving heat source)

After developing the numerical model of EBW process for spot welding, in the current section model is further upgraded to simulate the moving electron beam during the EBW process. Heat source model is applied in the form of multiple load steps along the weld direction for a given time step size calculated from weld speed. Fig. 4.2 shows the temperature contours for a moving heat source with a welding speed of 600 mm/min, beam current 110 mA and the beam voltage 50 kV.

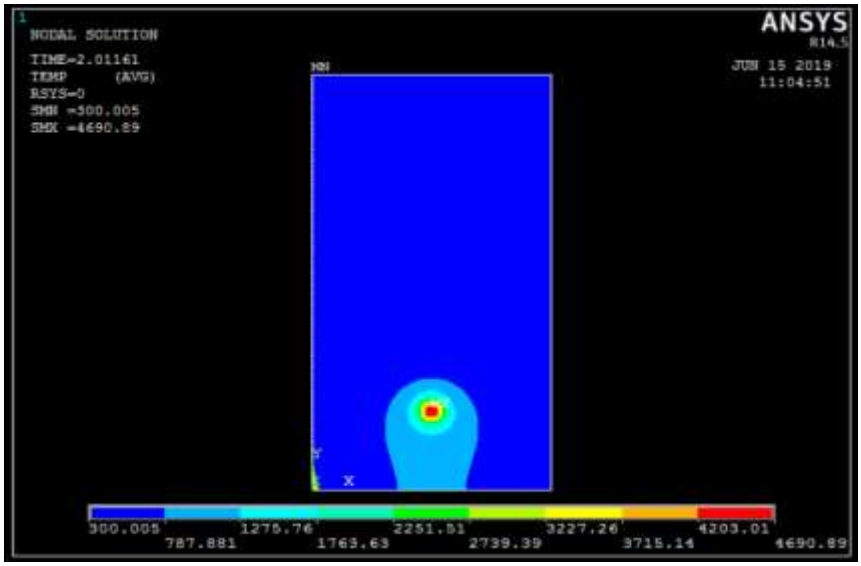

(a)

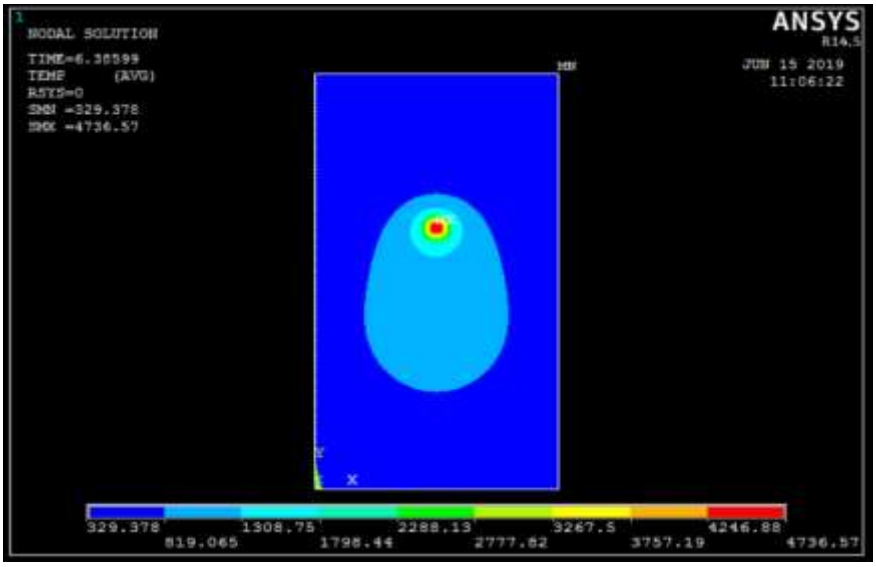

(b)

Fig. 4.2*Temperature distribution for moving heat source at time* ***(a)*** *2 seconds* ***(b)****6 seconds (current 110 mA, voltage 50 kV and weld speed 600 mm/ min).*

4.3 Validation of devdeloped numerical thermal model

Thermal model developed in the current work is compared with the experimental work carried out by Kanigalpula et al.[48]. The right side of the Fig. 4.3 (a-b) is an optical micrograph of the experimentally EBW welded plate while left side of the Fig. 4.3 (a-b) is showing cross section of numericallysimulatedtemperature profile.Numerically predicted values of BW and BP are shown by the horizontal and vertical extension of the red zone in the temperature contours. As shown in Fig. 4.3 (a) percentage error between the experimental and simulated results of BW, BP is 16.67 % and 5.17 % respectively. While, in Fig. 4.3 (b) there is an error of 18.92 % for BW and 2.34 % for BP respectively.

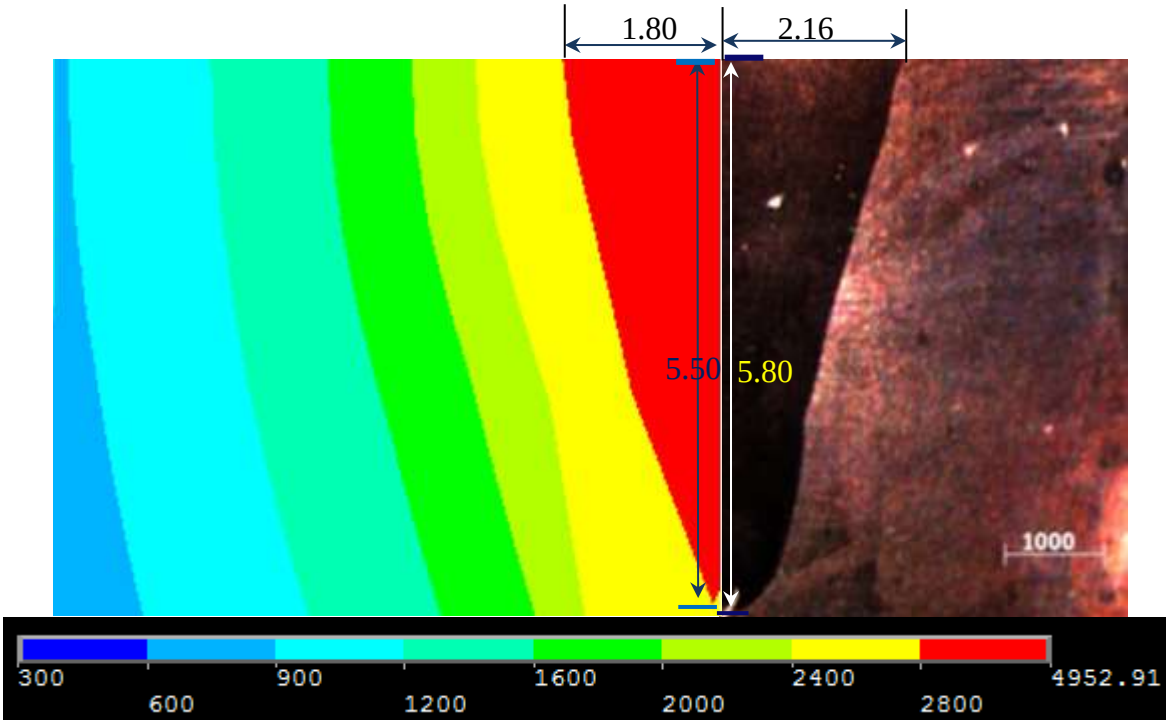

(a)

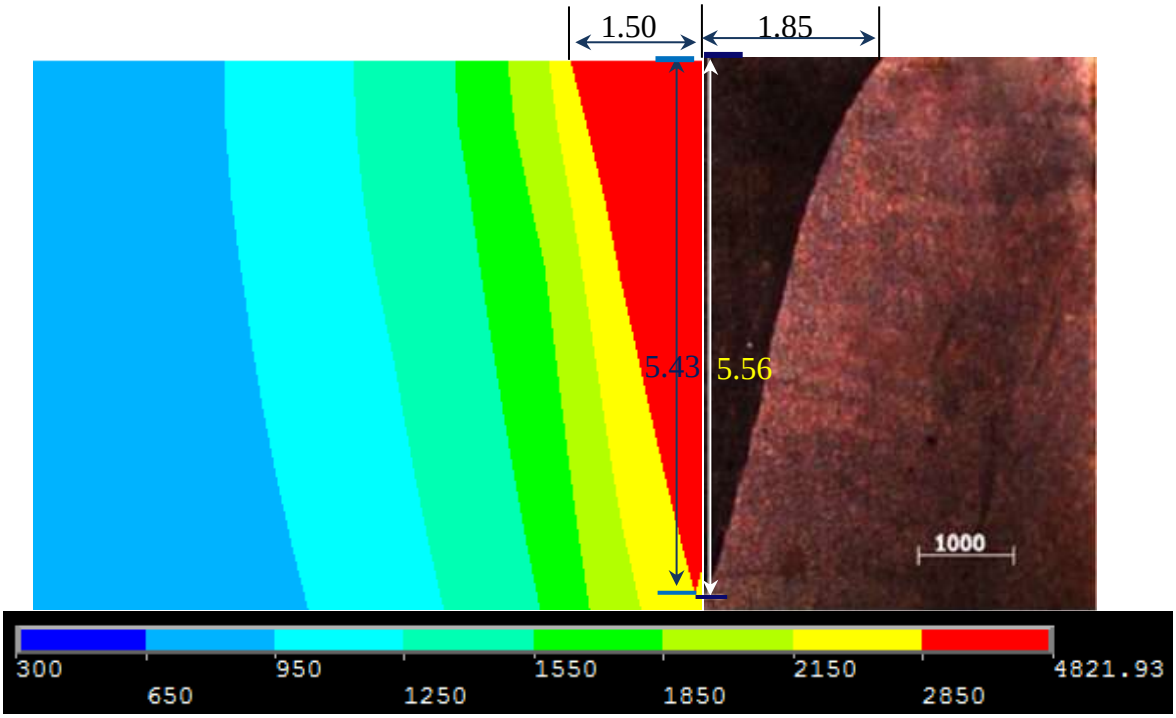

(b)

Fig. 4.3 *Compariosion between the experimentally and simulated values of bead width and bead penetration at various EBW input parameters* ***(a)*** *I= 110 mA,V = 60 kV, S = 1000 mm/min* ***(b)*** *I =90 mA, V= 55 kV,S = 800 mm/min*

4.4. Design of experiments

Parametric study of EBW process is carried out by using central composite design (CCD) method. The primarily aim for conducting parametric analysis is to study the effect of EBW input parameters viz. beam current (*I*), accelerating voltages (*V*) and the speed of the weld (*S*) and their interaction on EBW output responses viz. BW and BP. Table 4.1 shows the actual values of the various EBW input parameters used for carrying the numerical study. Range of these parameters was selected by running few trial experiments. A total of $2^3+2\times3+3=17$ combination of processes parameters was taken into account for these experiments.

Table 4.1 *Process parameters and their ranges used for EBW*

S. No	Inputs/unit	Symbol	Minimum value	Mid value	Maximum value
1.	Accelerating voltage (kV)	*V*	50	55	60
2.	Beam current (mA)	*I*	70	90	110
3.	Welding speed (mm/min.)	*S*	600	800	1000

Table 4.1 illustrates the comparative study between the numerically predicted results with the experimental results [48]. As shown in the table 4.1 the maximum percentage error between the experimental and simulated values of *BW, BP*are 20.85, 24.29 respectively.

Table 4.2 *Detailed plans of experiments with corresponding output responses*

S. No.	Accelerating voltage (kV)	Beam current (mA)	Welding speed (mm/min)	*Experimental Response*		*Numerical Response*		*% Error in BP (mm)*	*% Error in BW (mm)*
				BP_X (mm)	BW_X (mm)	*BP* (mm)	*BW* (mm)		
1	55	90	800	5.56	3.69	5.43	3	2.34	18.70
2	55	70	800	4.64	3	4.69	3.31	-1.08	-10.33
3	55	90	600	6.98	3.65	7.03	4	-0.72	-9.59
4	60	110	1000	5.8	4.32	5.5	3.6	5.17	16.67
5	55	110	800	6.26	4.35	6.03	3.8	3.67	12.64
6	50	70	1000	2.10	2.57	2.61	2.72	-24.29	-5.84
7	60	70	1000	3.92	3.86	3.81	3.72	2.81	3.63
8	60	70	600	4.64	2.94	4.72	2.74	-1.72	6.80
9	55	90	800	5.83	3.70	5.43	3	6.86	18.92
10	55	90	1000	4.93	3.98	4.83	3.15	2.03	20.85
11	50	110	1000	4.63	4.03	4.7	3.6	-1.51	10.67
12	50	90	800	3.62	3.98	3.4	3.3	6.08	17.09
13	60	90	800	5.5	3.7	5.36	3.35	2.55	9.46
14	60	110	600	9.1	4.97	9.24	5.06	-1.54	-1.81
15	55	90	800	6.07	3.59	5.43	3	10.54	16.43
16	50	110	600	8.22	4.8	8.17	4.7	0.61	2.08
17	50	70	600	4.91	3.19	4.02	3.01	18.13	5.64

As shown in the table 4.3 model-value of 0.018 and 0.007 for *BW* and *BWx* being less than 0.05 (significance level, α for 95 % confidence interval) imply that both models are significant. Highest percent contribution in deciding *BW* is by linear order term *I*. Simulated results shows that *S* and *S*I* as significant terms which is not reflected in the experimental study.

Table 4.3 *Analysis of variance for BW and BWx*

Source	***BW***			***BWx***		
	F-Value	**P-Value**	**% Contribution**	**F-Value**	**P-Value**	**% Contribution**
Model	5.470	0.018*		7.680	0.007*	
V	1.100	0.330	2.42	1.760	0.226	2.56
S	6.240	0.041*	13.71	0.740	0.418	1.08
I	23.330	0.002*	51.24	56.560	0.000*	82.29
V*V	0.000	0.981	0.00	0.390	0.552	0.57
S*S	1.470	0.265	3.23	0.230	0.643	0.33
I*I	1.250	0.301	2.75	0.090	0.770	0.13
V*S	0.870	0.381	1.91	4.080	0.083	5.94
V*I	0.140	0.715	0.31	0.500	0.503	0.73
S*I	11.130	0.012*	24.45	4.380	0.075	6.37

*Significant terms

ANOVA analysis of the simulated and experimental values of *BP* shows that all EBW input parameters plays a significant role in deciding *BP* (Table 4.4). Model terms in decreasing order of significance are *I, S, V* and V^2. Numerical study predicts 44.90 %, 32.49 %, 7.75 % and 4.45 % contribution of *I, S, V* and V^2 respectively. Same trend is observed for the experimental results with 44.85 %, 36.62 %, 7.08 % and 4.35 % contribution of *I, S, V* and V^2 respectively.

Table 4.4 *Analysis of variance for BP and BPx*

Source	***BP***			***BPx***		
	F-Value	**P-Value**	**% Contribution**	**F-Value**	**P-Value**	**% Contribution**
Model	17.400	0.001*		14.430	0.001*	
V	12.390	0.010*	7.75	9.320	0.019*	7.08
S	51.910	0.000*	32.49	48.240	0.000*	36.62

I	71.740	0.000*	44.90	59.080	0.000*	44.85
V*V	7.110	0.032*	4.45	5.730	0.048*	4.35
S*S	5.120	0.058	3.20	2.650	0.147	2.01
I*I	0.200	0.666	0.13	0.030	0.868	0.02
V*S	0.020	0.879	0.01	2.200	0.182	1.67
V*I	0.000	0.984	0.00	0.100	0.765	0.08
S*I	11.280	0.012*	7.06	4.380	0.075	3.32

*Significant terms

Regression equation for the experimentally obtained bead width, BW_X and simulated bead width, BW is given as:

$$BW_{X=} 14.9 - 0.565\ V - 0.01041\ S + 0.142\ I + 0.00444\ V\times V + 0.000002\ S\times S - 0.000135\ I\times I + 0.000207\ V\times S - 0.00072\ V\times I - 0.000054\ S\times I \quad (4.1)$$

$$BW = 4.9 - 0.044\ V - 0.00816\ S + 0.033\ I + 0.00084\ V\times V + 0.000007\ S\times S + 0.000628\ I\times I + 0.000073\ V\times S - 0.00087\ V\times I - 0.000091\ S\times I \quad (4.2)$$

Similarly, regression equation for the experimentally obtained bead depth, BP_X and simulated bead depth, BP are:

$$BP_X = -83.2 + 3.47\ V - 0.0357\ S + 0.092\ I - 0.0332\ V\times V + 0.000014\ S\times S + 0.000150\ I\times I + 0.000298\ V\times S + 0.00063\ V\times I - 0.000105\ S\times I \quad (4.3)$$

$$BP = -116.6 + 4.479\ V - 0.0158\ S + 0.025\ I - 0.03985\ V\times V + 0.000014\ S\times S + 0.000959\ I\times I + 0.000029\ V\times S - 0.00004\ V\times I - 0.000153\ S\times I \quad (4.4)$$

4.5 Effect of beam current

Fig. 4.4 (a-b) shows the variation of bead width and bead penetration with beam current. Bead width and bead penetration increases with the increase in beam current due to the fact that a higher current lead to increase in the number of the electrons that further results in high space charge inside the weld pool which leads to an increase in EBW output responses.

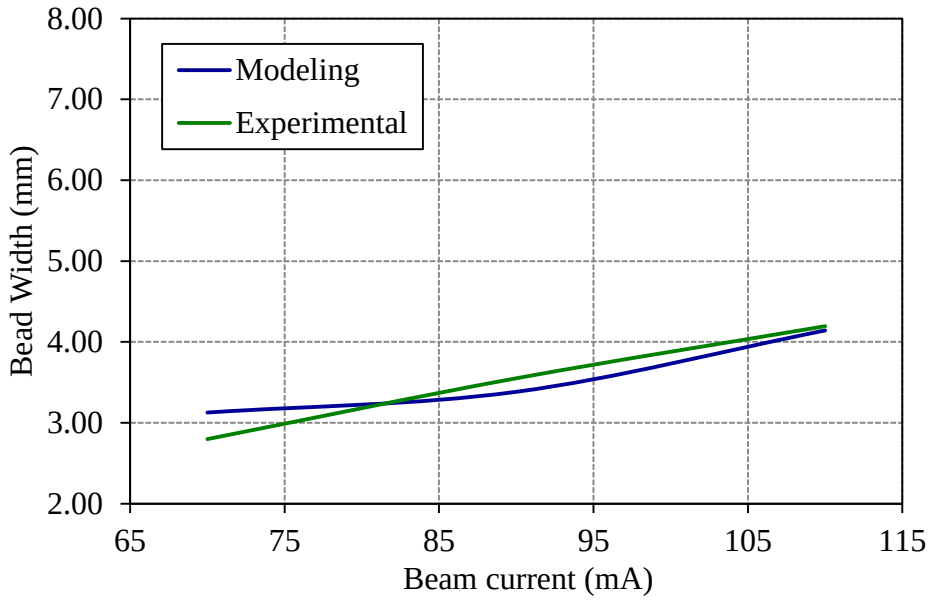

(a)

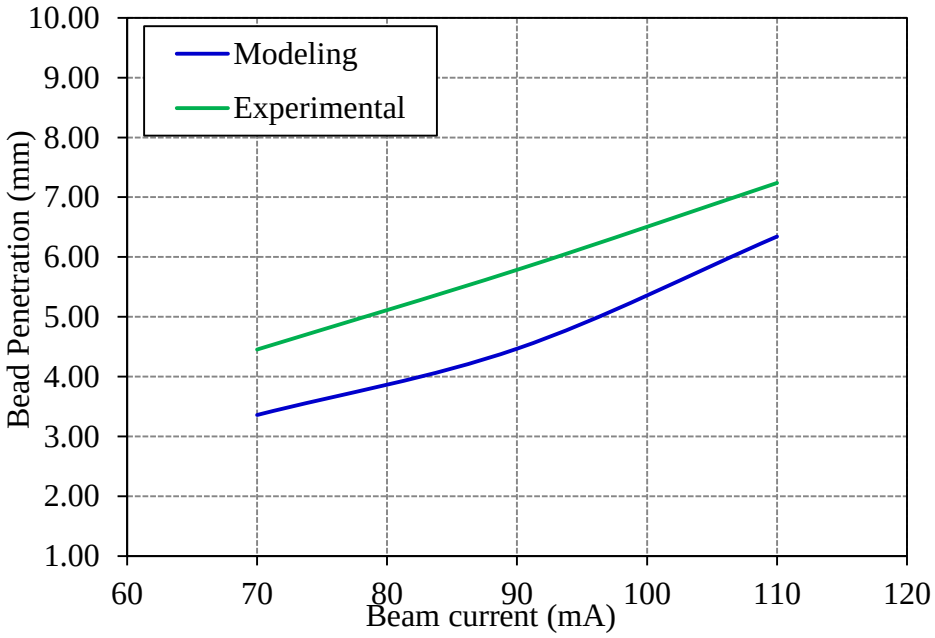

(b)

Fig. 4.4 *Effect of beam current on* ***(a)*** *bead width (BW, BW_X)* ***(b)*** *bead penetration (BP, BP_X)*

4.6 Effect of weld speed

As shown in Fig. 4.5 (a-b) both simulated as well as experimental values of bead width and bead penetration decreases with an increase in weld speed. This is due to the fact that as the weld speed increases, heat input per unit volume will decrease which lead to a decrease in bead width and bead penetration.

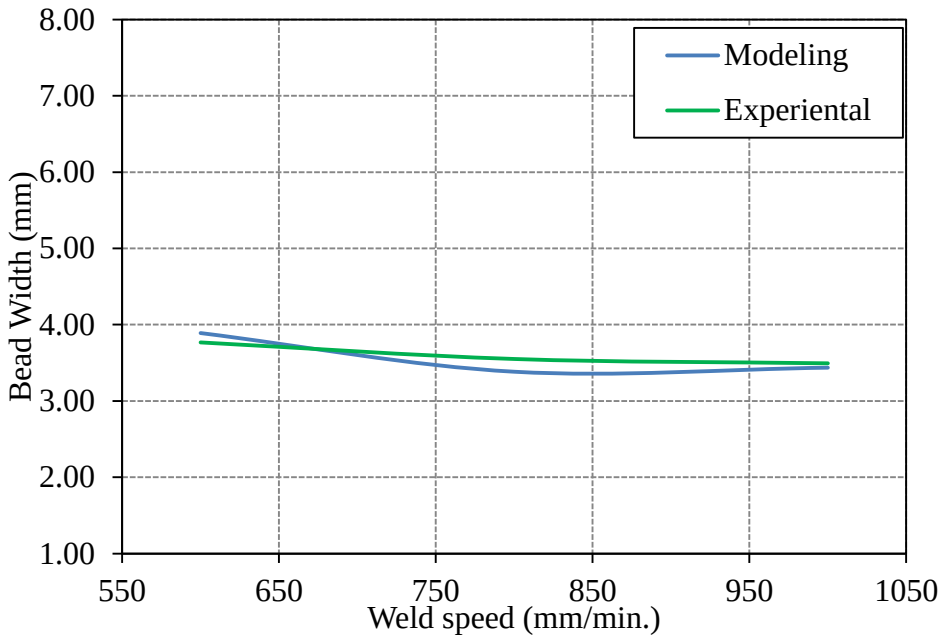

(a)

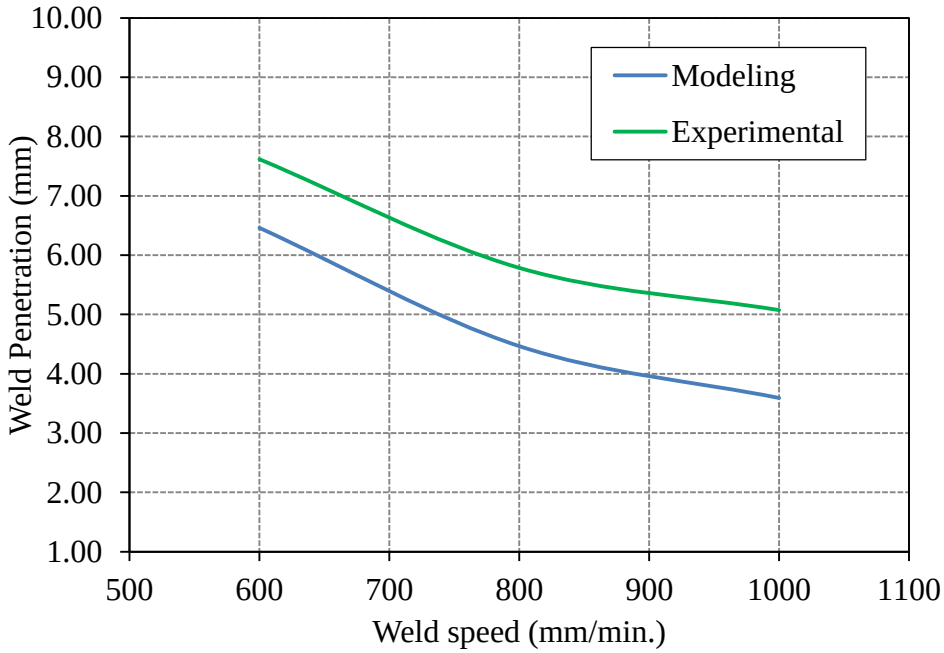

(b)

Fig. 4.5 *Effect of weld speed on* ***(a)*** *bead width (BW, BW_X)* ***(b)*** *bead penetration (BP, BP_X)*

4.7 Effect of voltage

Accelerating voltage is directly proportional to the kinetic energy of the beam electrons. As the voltage increased, kinetic energy of the electron will increase which results in an increase of bead width and bead penetration (Fig. 4.6 (a-b))

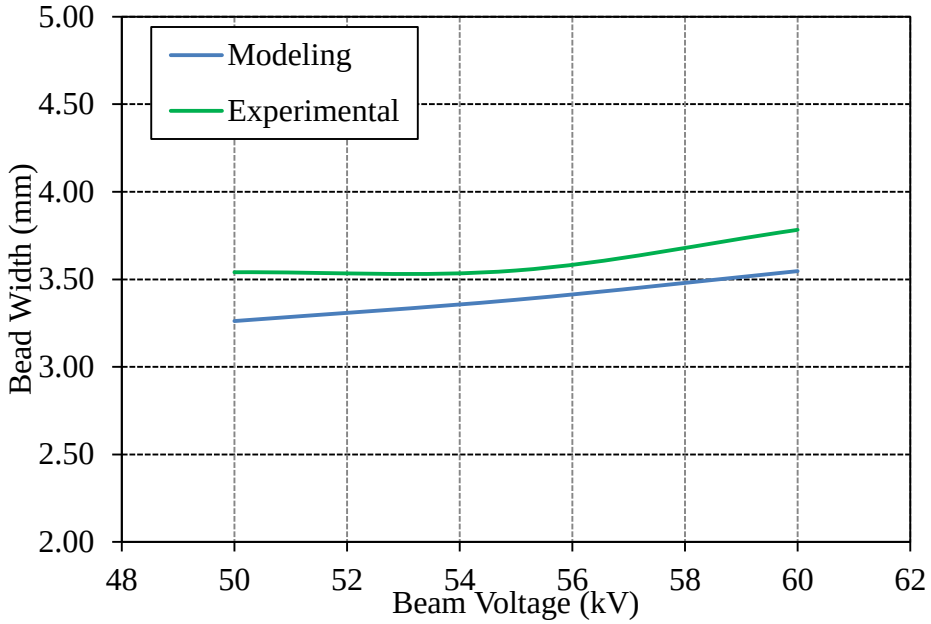

(a)

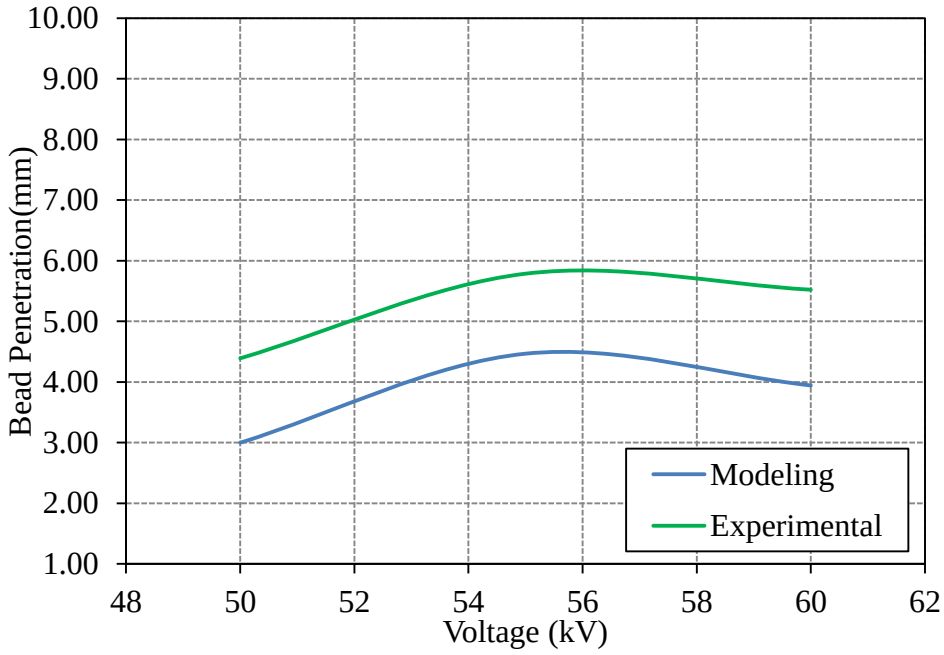

(b)

Fig. 4.6 *Effect of voltage on (a) bead width (BW, BW_X) (b) bead penetration (BP, BP_X)*

CHAPTER 5
CONCLUSION AND FUTURE SCOPE OF THE WORK

In the present work, a transient thermal analysis was carried out in Ansys14.5. A moving heat source model based on Gaussian and conical method has been implemented with the help of UDF to predict the temperature profile, *BP* and *BW* as the simulated results. In the present study shows that beam current has a major effect on EBW output responses followed by weld speed and voltage. As found out from simulation study percentage contribution of current, weld speed and voltage are 51.24 %, 13.71 % and 2.42 % respectively in determining bead width. Similarly, 44.90 %, 32.49 % and 7.75 % is the percentage contribution of current, weld speed and voltage in deciding bead penetration. Developed numerical model accurately predicts the output responses accept at very few experimental runs performed by Kanigalpulaet al.[19] on PH-CuCrZr alloy. The maximum percentage error between the experimental and simulated value of *BW*, *BP* is 20.85, 24.29 respectively.

Future work includes development of heat source model that can more accurately capture the size and shape of the weldment. Numerical model can further be developed to predict residual stresses generated during the EBW process. Also, numerical models can be developed to study the effect of various input parameters on the microstructure and mechanical properties such as hardness of the various zones generated during the welding.

REFERENCES

[1] Durashevich, Goran vladimirCvetkovski, and V. Jovanovich. "Effect of thermomechanical treatment on mechanical properties and electrical conductivity of a PH-CuCrZr alloy." Bulletin of Materials Science 25, no. 1 (2002): 59-62.

[2] Davis, Joseph R., ed. Copper and copper alloys. ASM international, 2001.

[3] Rotti, C., A. K. Chakraborty, I. Ahmed, G. Roopesh, M. Bandyopadhyay, M. J. Singh, Sejal Shah et al. "Development of PH-CuCrZr alloy for applications in Neutral Beams." In 2011 IEEE/NPSS 24th Symposium on Fusion Engineering, pp. 1-5, IEEE, 2011.

[4] Ihira, Ryota, HyoseongGwon, RyutaKasada, and Satoshi Konishi. "Improvement of tensile properties of pure Cu and PH-CuCrZr alloy by cryo-rolling process." Fusion Engineering and Design 109 (2016): 485-488.

[5] Feng, Hui, Haichang Jiang, Desheng Yan, and LijianRong. "Microstructure and mechanical properties of a PH-CuCrZr welding joint after continuous extrusion." Journal of Materials Science & Technology 31, no. 2 (2015): 210-216.

[6] Stütz, Markus, Diogo Oliveira, Matthias Rüttinger, NikolausReheis, Heinrich Kestler, and Norbert Enzinger. "Electron-beam welding of TZM sheets."In Materials Science Forum, vol. 879, pp. 1865-1869.Trans Tech Publications, 2017.

[7] Meleka, A. H. Electron-beam welding: principles and practice. Edited by Abdou Hanna Meleka. London: McGraw-Hill, 1971.

[8] Schiller, Siegfried, Ullrich Heisig, and Siegfried Panzer. Electron beam technology.John Wiley & Sons, 1982.

[9] Hemmer, H., and Ø. Grong. "Prediction of penetration depths during electron-beam welding." Science and technology of welding and joining 4, no. 4 (1999): 219-225.

[10] Rai, R., P. Burgardt, J. O. Milewski, T. J. Lienert, and T. DebRoy. "Heat transfer and fluid flow during electron-beam welding of 21Cr–6Ni–9Mn steel and Ti–6Al–4V alloy." Journal of Physics D: Applied Physics 42, no. 2 (2008): 025503.

[11] Tian, Yanhong, Chunqing Wang, Danyang Zhu, and Y. Zhou. "Finite element modeling of electron-beam welding of a large complex Al alloy structure by parallel computations." journal of materials processing technology 199, no. 1-3 (2008): 41-48.

[12] Weber, Charles Michael, E. R. Funk, and R. C. McMaster. "Penetration mechanism of partial penetration electron-beam welding."PhD diss., Ohio State University, 1970.

[13] Zhang, Ruihua, Ding Fan, and Seiji Katayama. "Electron-beam welding with activating flux." Transactions of JWRI 35, no. 1 (2006): 19-22.

[14] Węglowski, M. St, S. Błacha, and A. Phillips. "Electron-beam welding–Techniques and trends–Review." Vacuum 130 (2016): 72-92.

[15] Kaur, Aman, Colin Ribton, and W. Balachandaran. "Electron-beam characterisation methods and devices for welding equipment." Journal of materials processing technology 221 (2015): 225-232.

[16] Barreda, J. L., X. Azpiroz, and A. M. Irisarri. "Influence of the filler metal on the mechanical properties of Ti–6Al–4V electron-beam weldments." Vacuum 85, no. 1 (2010): 10-15.

[17] Sun, Z., and R. Karppi. "The application of electron-beam welding for the joining of dissimilar metals: an overview." Journal of Materials Processing Technology 59, no. 3 (1996): 257-267.

[18] Mladenov, G., K. Vutova, and S. Wojcicki. "Experimental investigation of the weld depth and thermal efficiency during electron-beam welding." Vacuum 51, no. 2 (1998): 231-233.

[19] Koleva, E., G. Mladenov, and K. Vutova. "Calculation of weld parameters and thermal efficiency in electron-beam welding." Vacuum 53, no. 1-2 (1999): 67-70.

[20] Mladenov, G., K. Vutova, and S. Wojcicki. "Experimental investigation of the weld depth and thermal efficiency during electron-beam welding." Vacuum 51, no. 2 (1998): 231-233

[21] Wei, P. S., and Y. T. Chow. "Beam focusing characteristics and alloying element effects on high-intensity electron-beam welding." Metallurgical Transactions B 23, no. 1 (1992): 81.

[22] Liu, Cheng-cai, and Jing-shan He. "Numerical analysis of thermal fluid transport behavior during electron-beam welding of 2219 aluminum alloy plate." transactions of nonferrous metals society of china 27, no. 6 (2017): 1319-1326

[23] Su, S. F., H. K. Lin, J. C. Huang, and N. J. Ho. "Electron-beam welding behavior in Mg-Al-based alloys." Metallurgical and Materials Transactions A 33, no. 5 (2002): 1461-1473.

[24] Rouquette, S., J. Guo, and Philippe Le Masson. "Estimation of the parameters of a Gaussian heat source model by the Levenberg–Marquardt method: Application to the electron-beam welding." International Journal of Thermal Sciences 46, no. 2 (2007): 128-138.

[25] Hemmer, H., and Ø. Grong. "Prediction of penetration depths during electron-beam welding." Science and technology of welding and joining 4, no. 4 (1999): 219-225.

[26] Elmer, J. W., W. H. Giedt, and T. W. Eagar. "The transition from shallow to penetration depth during electron-beam welding." Welding journal 69, no. 5 (1990): 167s-175s

[27] Ho, Ching-Yen, Mao-Yu Wen, and Yi-Chwen Lee. "analytical solution for three-dimensional model predicting temperature in the welding cavity of electron beam." no. 82, no. 3 (2007): 316-320.

[28] Turygin, Yuri, Milan Marônek, and Yuliya Zubkova. "investigation of the electron-beam positioning accuracy at electron-beam welding." procedia engineering 149 (2016): 489-494.

[29] Lacki, Piotr, Konrad Adamus, KwirynWojsyk, and Marcin Zawadzki. "Numerical analysisof electron-beam welding process of Inconel 706 sheets."In Key Engineering Materials, vol. 473, pp. 540-547.Trans Tech Publications, 2011.

[30] Lacki, Piotr, and Konrad Adamus. "Numerical analysisof the electron-beam welding process." Computers & Structures 89, no. 11-12 (2011): 977-985.

[31] Ferro, Paolo, Andrea Zambon, and Franco Bonollo. "Investigation of electron-beam welding in wrought Inconel 706—experimental and numerical analysis." Materials Science and Engineering: A 392, no. 1-2 (2005): 94-105.

[32] Lacki, Piotr, Konrad Adamus, and PawełWieczorek. "Theoretical and experimental analysis of thermo-mechanical phenomena during electron-beam welding process." Computational Materials Science 94 (2014): 17-26.

[33] Lundbäck, Andreas, and Henrik Runnemalm. "Validation of three-dimensional finite element model for electron-beam welding of Inconel 718." Science and Technology of Welding and Joining 10, no. 6 (2005): 717-724.

[34] Denlinger, Erik R., Jarred C. Heigel, and Panagiotis Michaleris. "Residual stress and distortion modeling of electron-beam direct manufacturing Ti-6Al-4V." Proceedings of the Institution of Mechanical Engineers, Part B: Journal of Engineering Manufacture 229, no. 10 (2015): 1803-1813.

[35] Patidar, Sunil, and DheerajSoni. "a review paper on comparative study of dissimilar metal welded joint using nickel as base material":(2018)

[36] Gery, D., H. Long, and P. Maropoulos. "Effects of welding speed, energy input and heat source model distribution on temperature variations in butt joint welding." Journal of materials processing technology 167, no. 2-3 (2005): 393-401.

[37] Chiumenti, Michèle, M. Cervera, NargesDialami, Bin Wu, L. Jinwei, and C. Agelet de Saracibar. "Numerical modeling of the electron-beam welding and its experimental validation." Finite Elements in Analysis and Design 121 (2016): 118-133.

[38] Rai, R., T. A. Palmer, J. W. Elmer, and T. Debroy. "Heat transfer and fluid flow during electron-beam welding of 304L stainless steel alloy." Weld. J 88, no. 3 (2009): 54-61.

[39] Luo, Yi, Guoqiang You, Hong Ye, and Jinhe Liu. "Simulation on welding thermal effect of AZ61 magnesium alloy based on three-dimensional modeling of vacuum electron-beam welding heat source model." Vacuum 84, no. 7 (2010): 890-895.

[40] ZHANG, Bing-gang, W. A. N. G. Ting, Xiao-hui DUAN, Guo-qing CHEN, and Ji-cai FENG. "Temperature and stress fields in electron-beam welded Ti-15-3 alloy to 304 stainless steel joint with copper interlayer sheet." transactions of nonferrous metals society of china 22, no. 2 (2012): 398-403.

[41] Trushnikov, D. N., and G. L. Permyakov. "Numerical analysisof electron-beam welding with beam oscillations." In IOP Conference Series: Materials Science and Engineering, vol. 177, no. 1, p. 012085. IOP Publishing, 2017.

[42] Tong, H., and W. H. Giedt. "dynamic interpretation of electron-beam welding." weld j 49, no. 6 (1970): 259.

[43] Ahmad, M., J. I. Akhter, M. Akhtar, M. Iqbal, E. Ahmed, and M. A. Choudhry. "Microstructure and hardness studies of the electron-beam welded zone of Hastelloy C-276." Journal of Alloys and Compounds 390, no. 1-2 (2005): 88-93.

[44] Kawamura, Yoshihito, Shinya Kagao, and YasuhideOhno. "Electron-beam welding of Zr-based bulk metallic glass to crystalline Zr metal." Materials Transactions 42, no. 12 (2001): 2649-2651

[45] Jang, Inkook, Susan B. Sinnott, Daniel Danailov, and Pawel Keblinski. "Molecular dynamics simulation study of carbon nanotube welding under electron-beam irradiation." Nano Letters 4, no. 1 (2004): 109-114.

[46] Jaypuria, Sanjib, VikasSheokand, Dilip Kumar Pratihar, and M. N. Jha. "Finite Element Analysis to Determine Residual Stress in Electron Beam Welding of CuCrZr alloy Plates and Experimental Validation." Materials Today: Proceedings 5, no. 9 (2018): 19321-19329.

[47] Shanmugam, N. Siva, G. Buvanashekaran, and K. Sankaranarayanasamy. "Some studies on temperature distribution modeling of laser butt welding of AISI 304 stainless steel sheets." In Proceedings of World Academy of Science, Engineering and Technology, no. 79, p. 1088.World Academy of Science, Engineering and Technology (WASET), 2013.

[48] Kanigalpula, P. K. C., D. K. Pratihar, M. N. Jha, J. Derose, A. V. Bapat, and A. Rudra Pal. "Experimental investigations, input-output modeling and optimization for electron-beam welding of Cu-Cr-Zr alloy plates." The International Journal of Advanced Manufacturing Technology 85, no. 1-4 (2016): 711-726

[49] Cheong, Yaw Peng, and Ritu Gupta. "Experimental design and analysis methods for assessing volumetric uncertainties." SPE Journal 10, no. 03 (2005): 324-335.

report

ORIGINALITY REPORT

14%	5%	11%	7%
SIMILARITY INDEX	INTERNET SOURCES	PUBLICATIONS	STUDENT PAPERS

PRIMARY SOURCES

1	Sanjib Jaypuria, Vikas Sheokand, Dilip Kumar Pratihar, M.N. Jha. "Finite Element Analysis to Determine Residual Stress in Electron Beam Welding of CuCrZr alloy Plates and Experimental Validation", Materials Today: Proceedings, 2018 Publication	1%
2	P. K. C. Kanigalpula, D. K. Pratihar, M. N. Jha, J. Derose, A. V. Bapat, A. Rudra Pal. "Experimental investigations, input-output modeling and optimization for electron beam welding of Cu-Cr-Zr alloy plates", The International Journal of Advanced Manufacturing Technology, 2015 Publication	1%
3	Submitted to Nilai University College Student Paper	1%
4	Encyclopedia of Thermal Stresses, 2014. Publication	<1%
5	"Lasers Based Manufacturing", Springer	